Materials Science & Engineering A 642 (2015) 57–64

Contents lists available at ScienceDirect

Materials Science & Engineering A

journal homepage: www.elsevier.com/locate/msea

Microstructure, mechanical properties and formability of friction stir processed interstitial-free steel

D.M. Sekban [a], O. Saray [b], S.M. Aktarer [c], G. Purcek [d,*], Z.Y. Ma [e]

[a] Department of Naval Architecture and Marine Engineering, Karadeniz Technical University, Trabzon, Turkey
[b] Department of Mechanical Engineering, Bursa Technical University, Bursa, Turkey
[c] Department of Automotive Technology, RecepTayyip Erdogan University, Rize, Turkey
[d] Department of Mechanical Engineering, Karadeniz Technical University, Trabzon, Turkey
[e] Shenyang National Laboratory for Materials Science, Institute of Metal Research, Chinese Academy of Sciences, Shenyang, China

ARTICLE INFO

Article history:
Received 19 April 2015
Received in revised form
20 June 2015
Accepted 23 June 2015
Available online 27 June 2015

Keywords:
IF-steels
Friction stir processing
Grain refinement
Formability

ABSTRACT

The microstructure, mechanical properties and stretch formability of fine-grained (FG) interstitial-free steel (IF-steel) formed by friction stir processing (FSP) was investigated systematically. One-pass FSP drastically refined the microstructure with aid of dynamic recrystallization (DRX) mechanism during processing and formed volumetric defect free basin-like processed region (PR) with a mean grain size of 5 μm (initial grain size was 40 μm). This microstructural evolution brought about a considerable increase in both hardness and strength values of IF-steel without considerable decrease in ductility values. Also, strain hardening dominated deformation behavior was obtained with the FSPed samples as an essential property for the engineering application. Coarse-grained (CG) IF-steel demonstrated high formability with an Erichsen index (EI) of 2.88 mm. Grain refinement by FSP yielded very close EI value of 2.80 mm with increasing punch load (F_{EI}). Force–displacement curves obtained in each process conditions reflected a similar membrane straining regimes where samples uniformly thinned under biaxial tension loads with aid of strain hardening capability. The formation of FG microstructure by FSP reduced the roughness (orange peel effect) of the free surface of biaxial stretched sample by decreasing the non-uniform grain flow leading to the so-called orange peel effect. It is concluded that a good balance of strength, ductility and strain hardenability along with equivalence formability to CG condition can be achieved by FSP as a single step practical procedure.

1. Introduction

Friction stir processing (FSP) is a novel surface engineering technique developed based on the principles of friction stir welding (FSW) [1,2]. In FSP, a non-consumable rotating tool with a shoulder and pin is inserted into a metal plate and traversed through a direction of interest. Heat generated by the friction between rotating tool and metal surface locally softens the volume to be processed. By traversing the rotating tool, the material flowing around the pin and the tool shoulder undergoes severe plastic deformation and thermal exposure [3]. Mainly, plastic deformation with frictional heating upto 0.6–0.7 T_m leads to dynamic recovery (DRV) and dynamic recrystallization (DRX) assisted microstructural refinement [4–6]. In many cases, the FSP leads to transformation of the coarse-grained (CG) initial microstructure into equiaxed fine-grained (FG) and/or even ultra-fine grained (UFG) structure mostly consisting of high angle grain boundaries (HAGBs) [1–5,7]. On the other hand, dendritic structure of the as-cast alloys can be successively broken-up, and casting defects like solidification micro-porosities, cavities and inclusions are eliminated with FSP [6,7]. Furthermore, this method has been successfully used for producing metal matrix surface composites on plate-type samples. Incorporation of reinforcement components like ceramic particles, multi-walled carbon nanotubes into the metal matrix have been done with the aid of intense plastic deformation and stirring during FSP [1,2].

It can be said that microstructural investigations have been extensively undertaken for the FSPed materials. Given the potential technological advantages of this effective and flexible technology, several research efforts have been made to understand the mechanical response and engineering performance of the FSPed materials. To date, considerable attention has been paid especially to the light metals namely wrought and cast Al, Mg, Cu and Ti alloys [1,2,8]. It has been demonstrated in these studies that mechanical properties of CG metallic materials could be enhanced by microstructural refinement and re-organization [1,2,8]. Generally,

* Corresponding author. Fax: +90 462 325 5526.
E-mail address: purcek@ktu.edu.tr (G. Purcek).

http://dx.doi.org/10.1016/j.msea.2015.06.068
0921-5093/

enhanced hardness and strength can be achieved for variety of material groups according to Hall–Petch type strengthening [1,2,8,9]. Softening of the precipitation-hardenable Al alloys, on the other hand, was reported due to the coarsening and dissolution of the precipitates as a result of the heat generated during FSP [10,11]. A simultaneous increase in strength and ductility was achieved with FSPed as-cast alloys, i.e. Al–Si alloys, as a result of structural refinement and elimination of the casting defects and breakage of dendritic microstructure [6,12–14]. Also, as-cast Mg and Al alloys showed better superplasticity at lower deformation temperatures and higher strain rates after FSP [15–17]. It was also reported that room temperature formability of Al5052-H32 [18] and AZ31 [19,20] alloys was improved by FSP.

As looking at the literature, less attention has been given to the processing of body-centered cubic (BCC) steels by FSP despite their significant industrial applications. In limited studies, mainly microstructural evolution and texture formation of FSPed steels were investigated [3,21–24]. It has been reported that the microstructures of FSPed steels consisted of nearly equiaxed grains with the sizes of micron levels [3,25]. Also, hardness of FSPed steels increased in the nugget zone (NZ) compared to that of the base material [3,21–24]. The effect of microstructural evolution on the strength and ductility of the FSPed steels was rarely reported. In a recent study, it was shown that plain low carbon steel subjected to FSP under rapid water cooling brought about a higher strength with a considerably high ductility compared to the quenched counterpart [22].

In view of above, further investigations are needed to identify the mechanical properties of the FSPed steels in order to reveal possible advantages of FSP on the strength and ductility. To the author's best knowledge, on the other hand, the effect of FSP on the formability of steels has not been investigated yet. Therefore, the purpose of this study is to investigate systematically the effect of microstructural evolution by FSP on the strength, ductility and formability of single-phase ferritic steels (IF-steel). Furthermore, the formability of the FSPed IF-steel (as a model material) was evaluated. This study has a potential to become a base for other studies in the formability of FSP-induced materials to be performed in future.

2. Experimental procedure

Cold rolled and continuously annealed IF-steel sheets having the chemical composition of 0.004 wt% C, 0.012 wt% Si, 0.2 wt% Mn, 0.012 wt% P, 0.009 wt% S, 0.1 wt% Ti and balance Fe was used in this study. Samples with the dimensions of 200 mm × 60 mm × 2 mm were cut from the as-received CG sheets. They were subjected to one-pass FSP using a WC tool consisting of a convex shoulder having a diameter of 16 mm and a cylindrical pin with a diameter and length of 5 mm and 1 mm, respectively (Fig. 1). Tool rotation speed and processing speed was set at 800 rpm and 65 mm/min, respectively. The shoulder tilt angle was 3°, and the tool plunger downforce were kept constant at 7 kN. Processing temperature was determined with a thermocouple placed in the vicinity of the processing surface of a dummy sample. Peak temperature was determined to be 760–800 °C which is lower than that of ferrite–austenite transformation temperature (≈ 910 °C).

Scanning electron microscope (SEM) and optical microscope (OM) were used to observe the microstructure of IF-steel samples before and after FSP. The metallographic specimens were sectioned perpendicular to the process direction (Fig. 1) and then etched in 2% Nital for 20 s after standard metallographic preparation. In order to reveal the microstructural details, electron backscattering diffraction (EBSD) was also performed on the processing plane (Fig. 1).

Hardness measurements were performed using a Vickers micro-hardness tester under a load of 200 g and for 10 s dwell time (Fig. 1). Tensile properties were determined on dog bone-shaped specimens with gauge section of 0.8 mm × 3 mm × 26 mm at a strain rate of $5.4 \times 10^{-4}\ s^{-1}$. The tensile axis of the samples was oriented parallel to the processing direction (Fig. 1). At least three tests were conducted to check the repeatability of both hardness and tensile test results for each point.

Stretch formability tests before and after FSP were performed using the Erichsen test technique, which is a well-established standard for studying the formability under biaxial strain conditions. The Erichsen test specimens with the dimensions of 13 mm × 13 mm × 0.7 mm were sectioned from the FSPed zone (Fig. 1). Specimen surfaces were prepared by grinding and polishing before FSP to avoid crack initiation effect of tool scars. The tests were performed using a miniaturized Erichsen die system attached to an Instron 3220 universal testing machine with a punch speed of 0.01 mm s^{-1} without lubrication. The dimensions of test die were chosen as 25% of standard Erichsen test fixture according to ISO-EN 20482 (Fig. 1(b)). After the test, the Erichsen Index (EI) and the load (F_{EI}) corresponding to this index were determined. At least three tests were performed for each curve to check the repeatability of the test results.

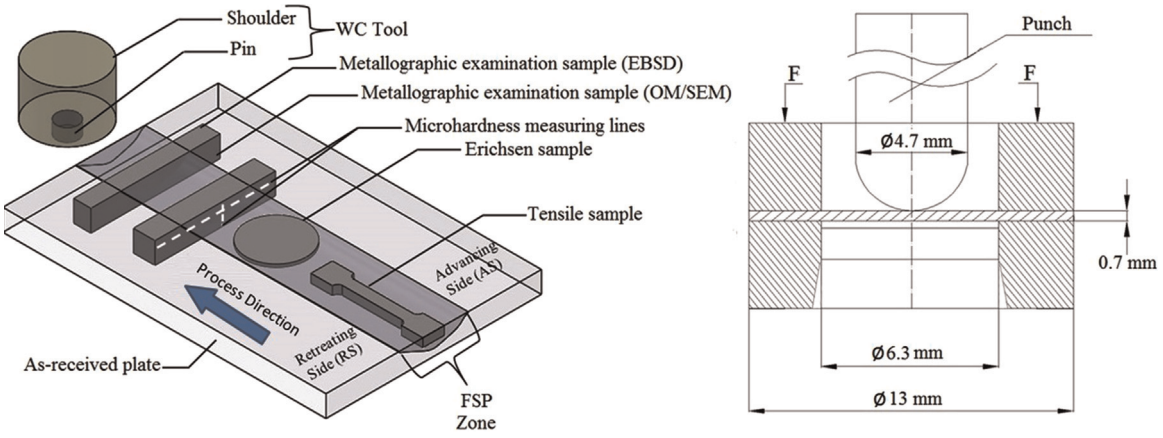

Fig. 1. (a) Schematic illustrations of the FSPed plate and the position of the specimens inside the FSPed zone. (b) Miniaturized Erichsen die set.

3. Results and discussion

3.1. Microstructure

FSP strongly affected the microstructure and formed volumetric defect free basin-like NZ having a depth of about 1.2 mm and a width close to diameter of the tool shoulder (16 mm) (Fig. 2(a)). Intense plastic deformation and complicated material flow around the stirring pin formed a NZ at the central parts of the PR with a darker contrast (Fig. 2(a)). Single phase ferritic microstructure having a mean grain size of 40 μm (Fig. 2(b)) was strongly refined and transformed into a fine-grained (FG) microstructure inside the NZ as a result of intense plastic deformation (Fig. 2(c)–(g)). It is evident from Fig. 2(c)–(d) that microstructure of the NZ were mainly composed of equiaxed grains with a mean size of about 5 μm. Also, both grain size and grain morphology are homogeneous through the zone. A transition region between the NZ and the unaffected zone known as thermo-mechanically affected zone (TMAZ) formed. Microstructure of the TMAZ mainly exhibited a band-like structure having strongly elongated ribbon-shaped grains (Fig. 2(e)–(g)). These microstructural characteristics were observed all around the boundary between the NZ and TMAZ. By the end of the TMAZ, grain morphology gradually became alike with that of as-received material. Hence, the TMAZ constituted both morphological and dimensional transformation region between the CG base material and FG processed material in the NZ.

EBSD map and grain size distribution histograms taken from the NZ are shown in Fig. 3(a). Grain morphology on the sheet plane of the FSPed region reflects a morphological transition from elongated grains to equiaxed grains through the center of the tool axis. The evaluation of the grains inside the NZ was also made by measuring the fraction of high angle grain boundaries (HAGBs) and low angle grain boundaries (LAGBs) and average misorientation angle (θ_{av}) (Fig. 3(b)–(d)). The grains under the effect of tool shoulder were extensively subdivided into the fine equiaxed subgrains with a mean grain size of about 2.5 μm (Fig. 3(b)). On the other hand, the HAGBs dominated microstructure at the central parts of the FSPed region where stirring took place (Fig. 3(a)). At this region, grains separated by the HAGBs were in the size range of 3–7 μm (average grain size is 5 μm). Also, mean grain size including both shoulder and pin affected regions were determined to be around 6 μm which is about 6 times finer than that of the as-received material. Such morphological and quantitative variations of the grain structure are attributed to the deformation- and temperature-induced grain subdivision mechanism [1–3].

Parent grains are subjected to intense shear deformation by rotating pin and transforms into the elongated grains (Fig. 3(a)) [1–3]. This becomes more pronounced towards the NZ due to accumulation of the shear deformation. As a result of plastic strain accumulation, dislocation density increases at the grain interior by the formation of dislocation clusters leading to increased internal energy [26,27]. In order to lower interior energy, dislocations are arranged to form LAGBs [26,27]. It was reported that the fraction of the LAGBs increases to high levels and spacing of these boundaries decreases with increasing shear deformation within the TMAZ [3]. Heat generated during FSP has been associated with microstructural evolution and transformation of the LAGBs into HAGBs [26,27]. Generally, continuous dynamic recrystallization (CDRX) is reported to be operative mechanism in the formation of HAGBs in warm deformation of high stacking fault energy materials like ferritic steels [3,22,28]. In this mechanism, new grains are not formed by a classical nucleation mechanism; the recrystallized

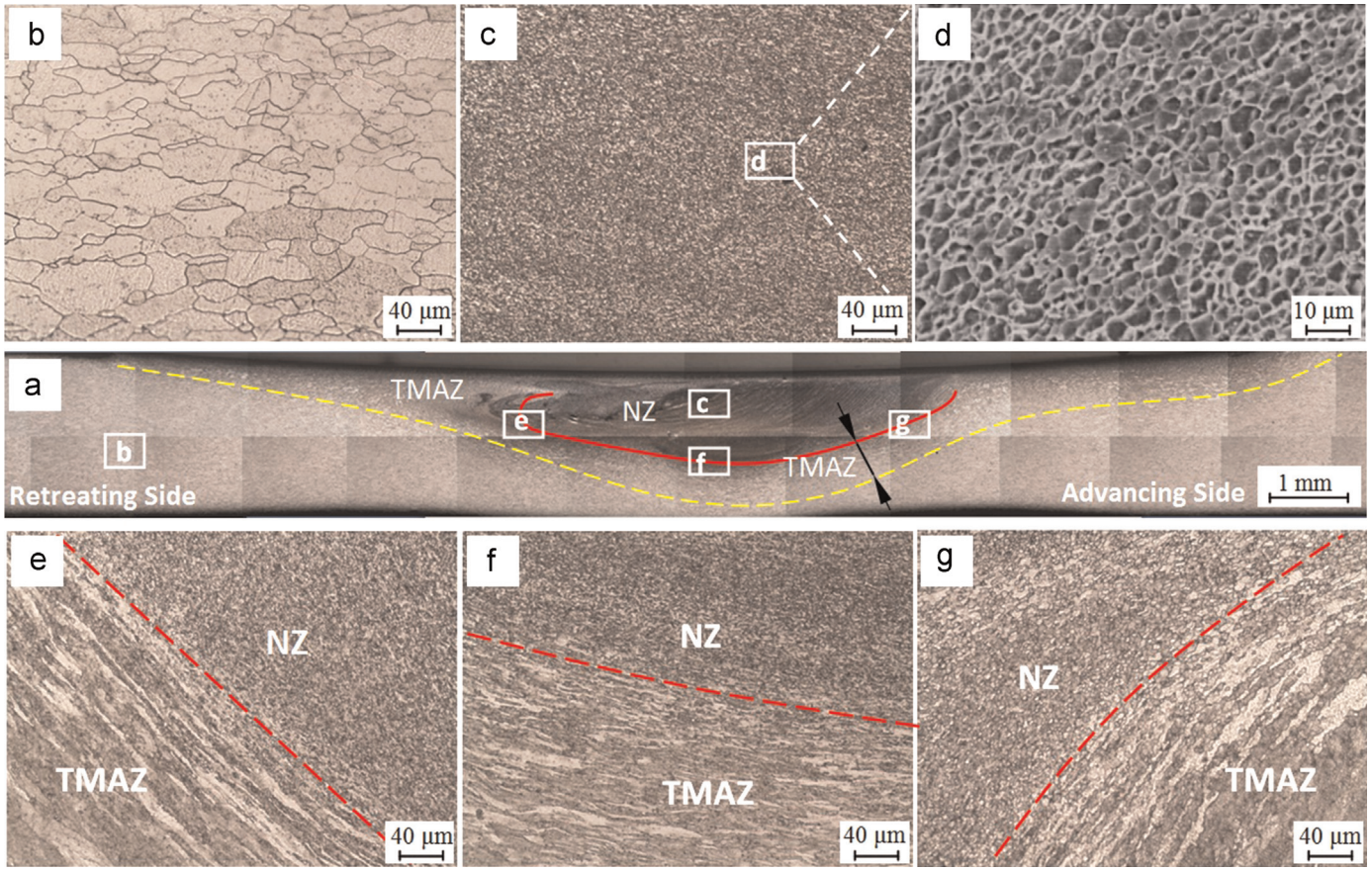

Fig. 2. (a) A general view of cross-section of the sample perpendicular to the advancing direction of the FSP. High magnification micrographs showing the: (b) un-processed region, (c)–(d) NZ optical and SEM micrographs and (e)–(g) transition zones between the NZ and TMAZ.

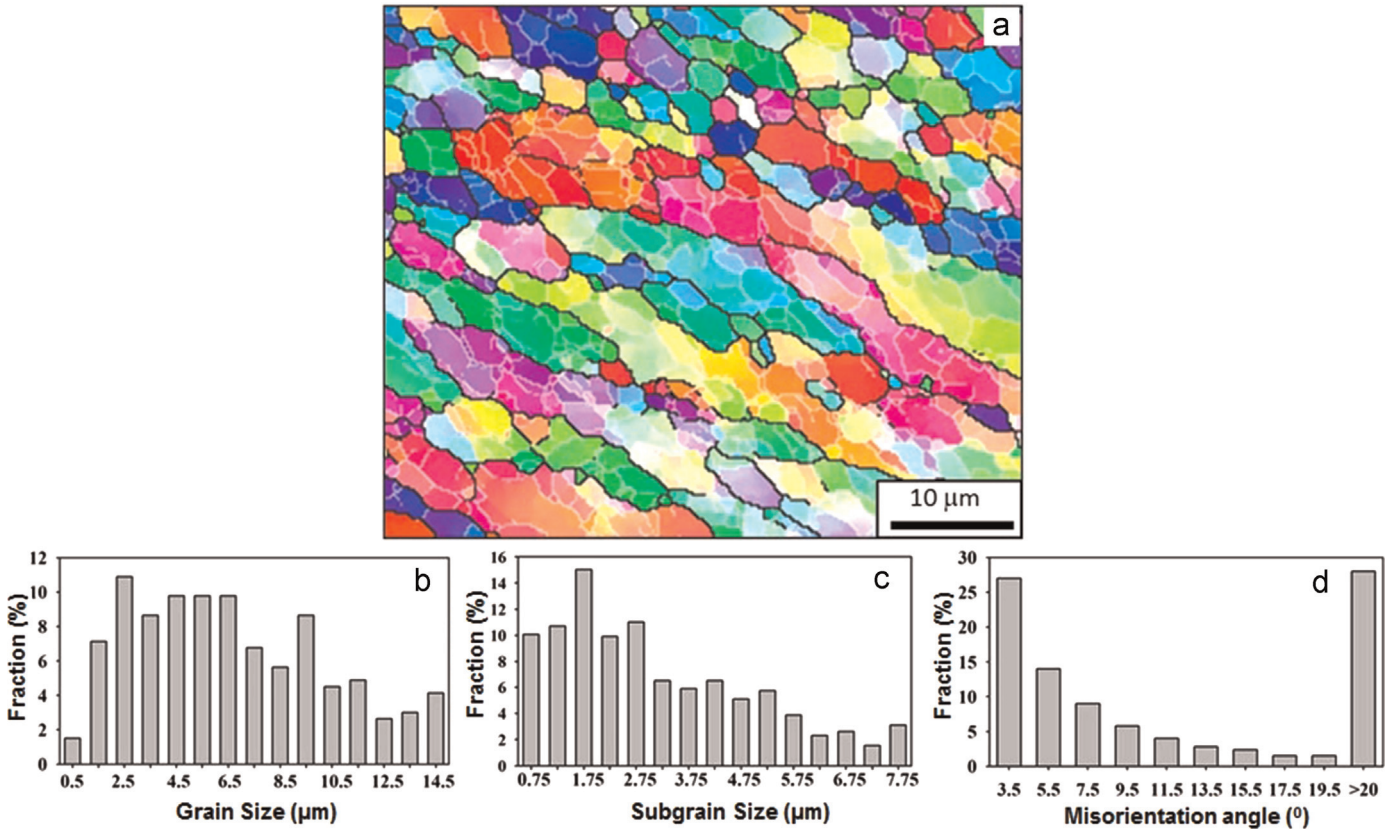

Fig. 3. (a) EBSD map of the NZ on the sheet plane and the histograms showing size distribution of the grains separated with (b) HAGBs, (c) LAGBs and (d) Misorientation angle distribution.

microstructure develops instead by the progressive transformation of subgrains into new grains, within the deformed original grains [28]. This mainly leads to the formation of homogenous microstructure having mainly equiaxed fine grains at the NZ where the highest level of frictional heat and plastic straining were achieved.

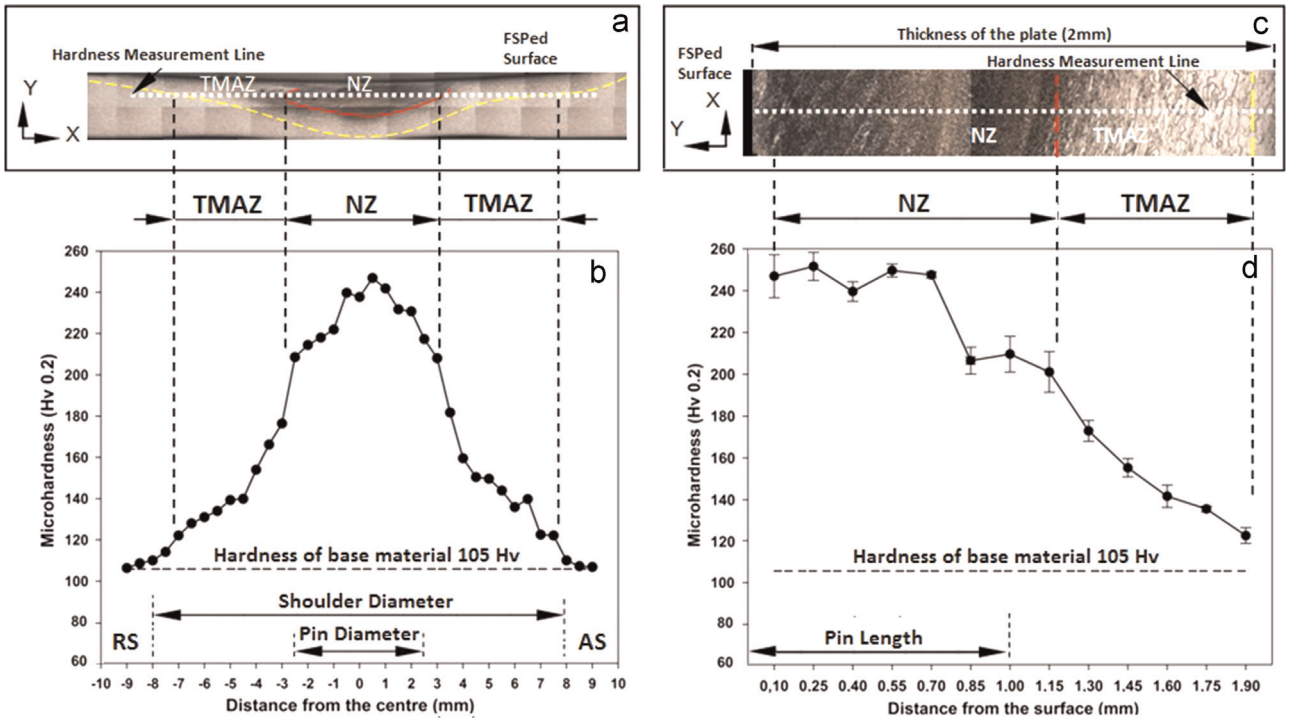

Fig. 4. Cross-sectional views and micro-hardness distributions of FSPed sample through (a)–(b) horizontal and (c)–(d) vertical directions.

3.2. Mechanical properties

Effect of microstructural evolution by FSP on the hardness of IF-steel was summarized in Fig. 4(a)–(d). In general, the hardness of CG sample increased considerably especially in the NZ by FSP. Horizontal hardness scan through the 0.7 mm offset to the sample surface revealed a nearly symmetrical hardness distribution by the tool axis. Peak hardness was reached at the center to about 250 Hv0.2. (Fig. 4(a)–(b)). The mean hardness of un-processed sample increased from 105 Hv0.2 to about 257 Hv0.2 through a depth of about 0.7 mm after FSP (Fig. 4(c)–(d)). After then, the hardness continuously decreased and approached to the value of base material towards the root of the NZ. Hardness distributions were more or less homogeneous with a variation of about ± 10 Hv0.2 within the NZ. However this trend changed with a sharp decrease by the end of the TMAZ (Fig. 4(b)). Such increase in hardness of the NZ may be considered as an expected result of the grain refinement. Also, an increase in dislocation density induced by intensive plastic deformation is also effective in the enhancement of hardness [1–3]. Variations in hardness values inside the NZ and TMAZ may be related to the microstructural alterations like complicated material flow, variations of straining levels and differences in the dynamic recrystallization rate through the NZ due to inhomogeneous cooling or heat flux within the sample [8].

The stress–strain curves of CG and FSPed FG IF-steel samples are shown in Fig. 5. The yield strength (σ_y), ultimate tensile strength (σ_{uts}), uniform elongation (ε_u), and elongation to failure (ε_f) taken from this curves are summarized in Table 1. As-received CG sample showed low strength and high elongation with a very large strain-hardening region (Fig. 5). The stress–strain curve of CG sample changed after FSP. The strain hardening region of the sample decreased after processing, and large portion of elongation took place without necking. Strength of CG steel was increased drastically by the effect of FSP. The σ_y and σ_{uts} of the CG steel increased from 134 MPa and 242 MPa to about 381 MPa and 401 MPa, respectively, after FSP. More importantly, the strengthening was achieved without a considerable decline of ductility, which is a crucial parameter considering the engineering applications of the steels. In CG state, the ε_u and ε_f were 24.4% and 52.2%, respectively. After FSP, the ε_f value decreased to about to 39.1%. However considerably high uniform elongation of about 16% was still retained after FSP. Such improvement in strength of the FSPed sample is assumed to be primarily from the considerably refined microstructure leading to grain size strengthening (Fig. 2(c)) [25]. In many cases, it has been shown that LAGBs are evident in the microstructure of the FSPed metals [2,3]. Hence, LAGBs may also contribute to strengthening of the FSPed sample [26]. Decrease in ductility with FSP is related to the strain hardening parameters. In the CG sample, strain hardening coefficient (K) and strain hardening exponent (n) were determined to be 380 MPa and 0.25, respectively. In the case of FSPed steel, they were determined to be 580 MPa and 0.12, respectively. Lower strain hardening coefficient of the FSPed sample mainly indicates a decreasing contribution of the dislocation interaction on the strength during the plastic deformation. This led to formation of plateau shaped stress–strain curve showing a slight stress increase with uniform straining (Fig. 5). Lower strain hardenability of the FSPed steel may be related to its refined grain size. It is well known that strain hardening mainly occurs with interactions of the dislocation with each other or other microstructural obstacles like HAGBs [5,8]. Grain refinement decreases the HAGB spacing leading to decrease in dislocation free path. Hence dislocation accumulation to initiate a micro-crack requires lower plastic deformation due to higher number of grains contributing to this process. Hence macroscopic necking starts more easily at smaller plastic strains leading to lower uniform elongation in FG and UFG materials.

Table 1
Mechanical properties of as-received CG and FSPed FG IF-steel samples.

Condition	σ_y (MPa)	σ_{UTS} (MPa)	ε_u, (%)	ε_f (%)	K (MPa)	n
As-received (CG)	134 ± 04	242 ± 06	23.4 ± 0.3	52.2 ± 3.4	380	0.25
FSPed (FG)	381 ± 09	401 ± 11	16.5 ± 0.8	39.1 ± 2.1	580	0.12

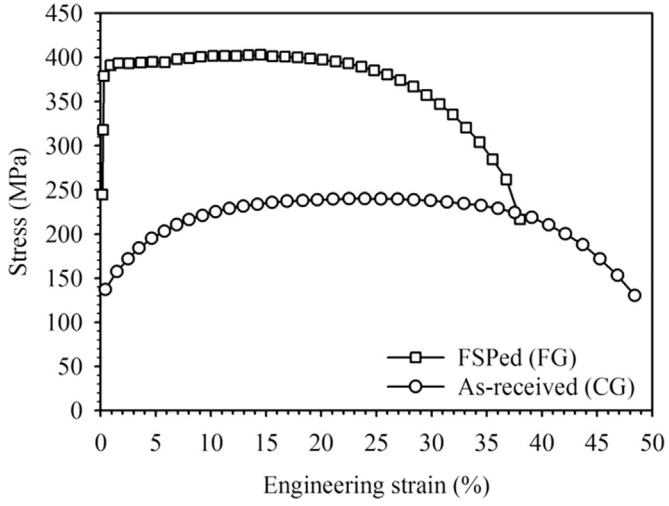

Fig. 5. Room temperature stress–strain curves of the as-received CG and FSPed FG IF-steel samples.

3.3. Stretch formability

Load (F)–displacement (X) curves produced from the Erichsen tests are shown in Fig. 6. Values of Erichsen index (EI) and punch load at EI (F_{EI}) determined from F–X curves are given in Table 2. It is seen from F–X curves that deformation of CG and FG samples takes place in several stages under biaxial stresses via Erichsen tests [29–31]. In order to distinguish these stages from each other, the first order derivative of the punch load (F) with respect to the displacement (X) was calculated, and the dF/dX–X curves were depicted in Fig. 6. The main characteristics and deformation behavior of the Erichsen tested samples were investigated in several studies [29–32]. Mainly, deformation of the sample starts with an elastic bending stage fallowed by local surface micro yielding and yield surface propagation. After yield surface propagation, sample

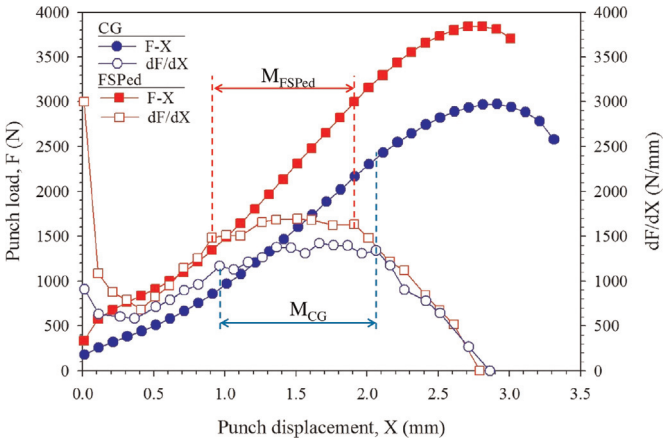

Fig. 6. Punch load (F)–punch displacement (X) curves and dF/dX – X curves of as received and FSP processed IF-steel.

Table 2
Erichsen Index (EI) and punch force (F_{EI}) of CG and FSPed IF-steel samples.

Condition	Erichsen index (EI) (mm)	Load at Erichsen index (F_{EI}) (N)
As-received (CG)	2.90 ± 0.1	2995 ± 53
Processed (FG)	2.80 ± 0.1	3804 ± 67

deforms with plastic bending. Plastic bending is followed by membrane straining where the sample thins under the effect of biaxial tension stresses acting on the dome wall. Because of strain accumulation within the membrane straining regime, deformation becomes local with the mechanism of the plastic instability and necking. Considering the deformation stages of the Erichsen test, one can conclude that membrane straining regime is the most distinguishing stage determining the formability and/or Erichsen index of the sample. This stage was found to be strongly depending on the strain hardening capability of the samples. As an expected result, onset of plastic instability is shifted to higher punch displacements by more decent in strain hardening capability leading to higher Erichsen index and better formability. In this point of view, greater emphasis were given to the membrane straining regime of the CG and FSPed samples in order to understand effect of the microstructural variations on the deformation behavior and formability of the IF-steel.

Biaxial tension deformation of the CG sample took place with the aid of strain hardening leading to the formation of a membrane straining regime designated as "M_{CG}" in Fig. 6. In this regime, the dF/dX remains nearly constant with increasing punch displacement. This mainly indicates that strain hardening capability of the CG sample compensated the possible load decreases due to the thinning of the sample under biaxial tension loads [30,31]. This stage continued till deformation localization formed

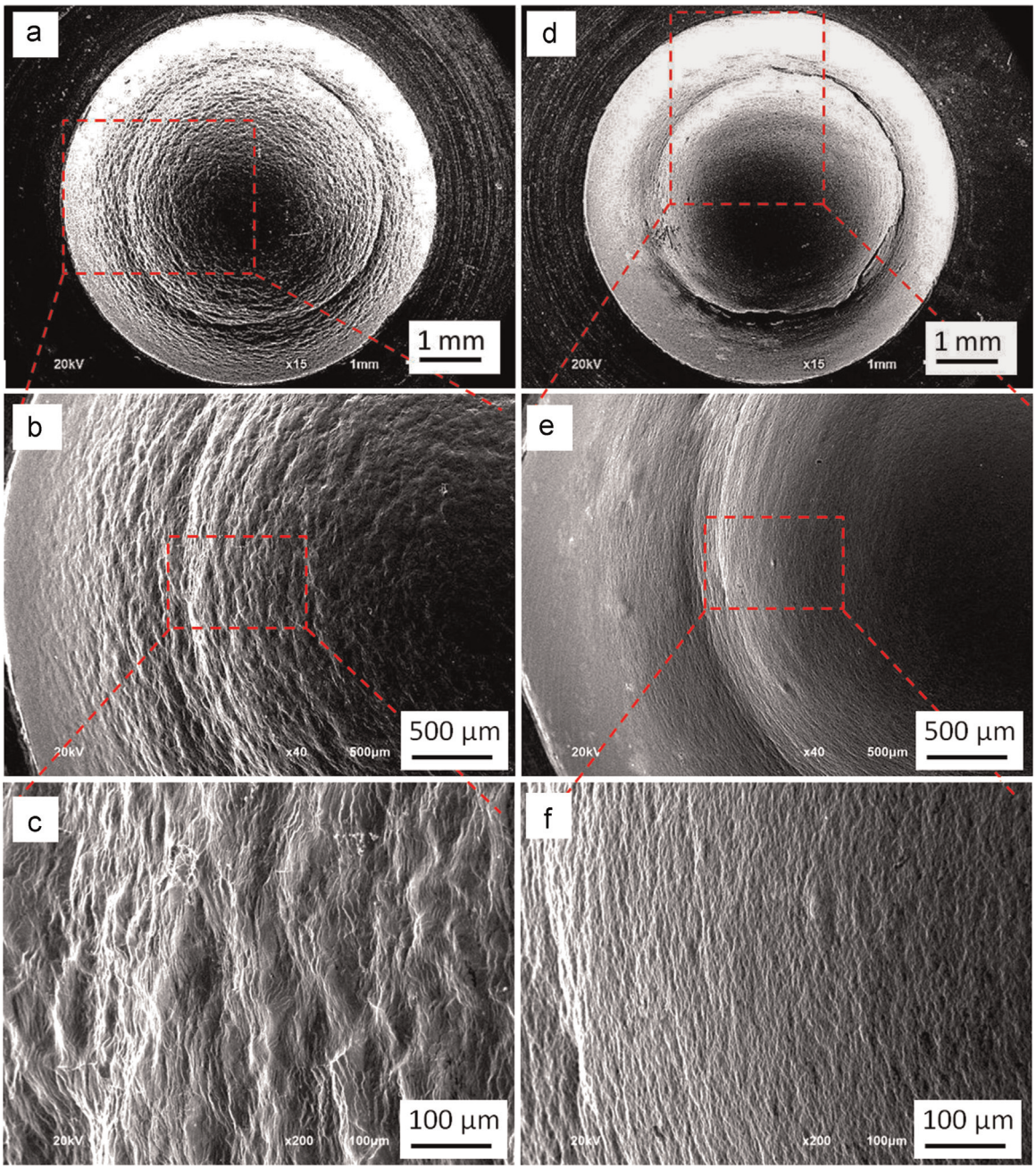

Fig. 7. Dome free surface appearances of the Erichsen tested samples in: (a)–(c) CG and (d)–(f) FSPed conditions.

with neck formation. By the formation of the necking, the dF/dX decreases continuously due to the localized thinning of the sample and reached to the zero at the EI of 0.80. No considerable change was seen in the deformation behavior of the sample after FSP. The punch displacement within the membrane straining regime (M_{FG}) was slightly contracted compared to the CG counterpart (Fig. 6). This may be due to the more or less negative effect of FSP on the strain hardening behavior of the IF-steel leading to lower strain hardening exponent (Table 1). This behavior also affected the EI values. The EI of the CG and FSPed IF-steel were determined to be 2.88 mm to 2.80 mm, respectively. Narrower membrane straining region of the FSPed samples turned out early initiation of the cracks after lower punch displacement led to lower EI. On the other hand, high strength of the FSPed samples increased the required load (punch load) for plastic deformation during Erichsen test. From Table 2, the F_{EI} was determined as 2995 N for the CG condition. This value increased to about 3804 N after FSP.

Dome free surface appearances of the Erichsen tested samples are represented in Fig. 7. Initially polished dome free surface of the CG sample roughened extensively during stretching, which resulted in an "orange peel effect" (Fig. 7(a)–(c)) [30,31]. The roughening with orange peel effect can be attributed to the strain differences between the neighbor grains due to the crystallographic orientation variations [33]. Such strain differences between the neighbor grains lead to the formation of a grainy appearance of plastically deformed free surface due to the formation of surface level differences between the neighboring grains [30,31]. FSP strongly affected the surface appearance of the samples. Dome free surface of the FSPed sample was smoother than that of the CG counterpart (Fig. 7(a)–(b)). Decrease in surface roughness after FSP can be attributed to the refinement of the grains inside the surface layer. During stretching, grains deform in particular slip systems. Strain incompatibilities between a grain and its neighbor causes grains to move normal to the surface. As an expected result, grain refinement increases the number of the grains at the free surface. This lowers the area of the grains on the free surface of the samples leading to the formation of a smoother free surface by decreasing the normal movement of the grain surfaces relative to each other during stretching.

Previous studies on the formability of the UFG materials revealed that equiaxed grain morphology with a grain size larger than 7 μm is required to obtain a good formability with uniform thinning of the sample [30,31]. This was achieved by employing a proper annealing procedure for UFG materials produced by ECAE processing in order to get both high strength and uniform formability. Annealing of the severely deformed structure decreased dislocation density and increased the grain size which eliminates deformed microstructure leading to early cracking under biaxial stretching due to the stress concentration [30,31]. On the other hand, employing FSP to refine the microstructure satisfied these requirements by dynamic recrystallization assisted microstructural refinement leading to formation of equiaxed grains with a mean grain sizes between 5 and 10 μm as in the case of present study (Fig. 3). This indicates the effectiveness of the FSP, as the one-step procedure to produce materials with optimized strength with high uniform formability.

4. Conclusions

In the present study, the effect of friction stir processing (FSP) on the microstructure, mechanical properties and biaxial stretch formability of BCC IF-steel was investigated. The main results and conclusions of this study can be summarized as follows:

1. A fine grained microstructure having mean grain size of 5 μm were obtained from the CG (grain size: 40 μm) IF-steel with one-pass FSP. Such grain refinement leads to a significantly enhancement in strength values without notably sacrificing the elongation to failure.
2. The CG samples demonstrated high formability and deform uniformly under biaxial loading conditions. Grain refinement via FSP had no considerable effect on the stretch formability and deformation behavior under biaxial tension loading conditions. This attributed to the strain hardening dominated uniaxial deformation behavior because dynamic recrystallization assisted grain refinement mechanism leads to the formation of equiaxed grains separated by both HAGBs and LAGBs.
3. The surface quality of the stretched samples was improved by grain refinement via FSP, and orange peel effect on the dome free surface of the CG sample was considerably reduced with the FG formation.
4. FSP can be considered as a practical, one-step tool to increase the effectiveness of the materials in engineering applications by means of optimized strength with high formability and lower orange-peel effect formation.

Acknowledgments

We would like to thank Dr. Tevfik Kucukomeroglu for his contributions on fixing the FSP set-up and help on performing the processes.

References

[1] R.S. Mishra, Z.Y. Ma, Mater. Sci. Eng. R 50 (2005) 1–78.
[2] Z.Y. Ma, Metall. Mater. Trans. A 39 (2008) 642–658.
[3] S. Mironov, Y.S. Sato, H. Kokawa, Acta Mater. 56 (2008) 2602–2614.
[4] C.G. Rhodes, M.W. Mahoney, W.H. Bingel, M. Calabrese, Scr. Mater. 48 (2003) 1451–1455.
[5] J.-Q. Su, T.W. Nelson, C.J. Sterling, Scr. Mater. 52 (2005) 135–140.
[6] M.L. Santella, T. Engstrom, D. Storjohann, T.Y. Pan, Scr. Mater. 53 (2005) 201–206.
[7] Z.Y. Ma, A.L. Pilchak, M.C. Juhas, J.C. Williams, Scr. Mater. 58 (2008) 361–366.
[8] R. Nandan, T. DebRoy, H.K.D.H. Bhadeshia, Prog. Mater. Sci. 53 (2008) 980–1023.
[9] C.I. Chang, C.J. Lee, J.C. Huang, Scr. Mater. 51 (2004) 509–514.
[10] Y. Sato, H. Kokawa, K. Ikeda, M. Enomoto, T. Hashimoto, S. Jogan, Metall. Mater. Trans. A 32 (2001) 941–948.
[11] G. Liu, L.E. Murr, C.S. Niou, J.C. McClure, F.R. Vega, Scr. Mater. 37 (1997) 355–361.
[12] Z.Y. Ma, S.R. Sharma, R.S. Mishra, Metall. Mater. Trans. A 37 (2006) 3323–3336.
[13] M. Tsujikawa, S. Chung, T. Morishige, L. Chiang, Y. Takigawa, S. Oki, K. Higashi, Mater. Trans. 48 (2007) 618–621.
[14] D. Zhang, M. Suzuki, K. Maruyama, Scr. Mater. 52 (2005) 899–903.
[15] R.S. Mishra, M.W. Mahoney, S.X. McFadden, N.A. Mara, A.K. Mukherjee, Scr. Mater. 42 (1999) 163–168.
[16] Z.Y. Ma, R.S. Mishra, M.W. Mahoney, Acta Mater. 50 (2002) 4419–4430.
[17] P. Cavaliere, P.P. De Marco, J. Mater. Process. Technol. 184 (2007) 77–83.
[18] S.H. Kang, H.-S. Chung, H.N. Han, K.H. Oh, C.G. Lee, S.-J. Kim, Scr. Mater. 57 (2007) 17–20.
[19] L.L. Hütsch, J. Hütsch, K. Herzberg, J.F. dos Santos, N. Huber, Mater. Design 54 (2014) 980–988.
[20] G. Venkateswarlu, D. Devaraju, M.J. Davidson, B. Kotiveerachari, G.R.N. Tagore, Mater. Design 45 (2013) 480–486.
[21] Y.C. Chen, K. Nakata, Mater. Charact. 60 (2009) 1471–1475.
[22] P. Xue, B.L. Xiao, W.G. Wang, Q. Zhang, D. Wang, Q.Z. Wang, Z.Y. Ma, Mater. Sci. Eng. A 575 (2013) 30–34.
[23] N. Yasavol, A. Abdollah-zadeh, M.T. Vieira, H.R. Jafarian, Appl. Surf. Sci. 293 (2014) 151–159.
[24] S.H. Aldajah, O.O. Ajayi, G.R. Fenske, S. David, Wear 267 (2009) 350–355.
[25] H. Fujii, L. Cui, N. Tsuji, M. Maeda, K. Nakata, K. Nogi, Mater. Sci. Eng. A 429 (2006) 50–57.
[26] N. Hansen, X. Huang, D.A. Hughes, Mater. Sci. Eng. A 317 (2001) 3–11.
[27] N. Hansen, Plastic behavior of metals: large strains, in: K.H. Jürgen Buschow, Robert W. Cahn, Merton C. Flemings, Bernard Ilschner, Edward J. Kramer, Subhash Mahajan, Patrick Veyssière (Eds.), Encyclopedia of Materials, Science and Technology,, Elsevier, Oxford, 2001, pp. 7040–7050.
[28] S. Gourdet, F. Montheillet, Acta Mater. 51 (2003) 2685–2699.

[29] M.P. Manahan, A.E. Browning, A.E. Argon, O.K. Harling, Miniaturized disc bend test technique development and application, the use of small-scale specimens for testing irradiated material, in: W.R. Corwin, G.E. Lucas (Eds.), The Use of Small-Scale Specimens for Testing Irradiated Material, ASTM, Albuquerque N. M., 1986.
[30] O. Saray, G. Purcek, I. Karaman, H. Maier, Metall. Mater. Trans. A 44 (2013) 1–13.
[31] O. Saray, G. Purcek, I. Karaman, H.J. Maier, Mater. Sci. Eng. A 619 (2014) 119–128.
[32] E. Fleury, J.S. Ha, Int. J. Press. Vessel. Pip. 75 (1998) 699–706.
[33] R. Becker, Acta Mater. 46 (1998) 1385–1401.